Turbulent magnetic dynamo excitation at low magnetic Prandtl number

Pablo D. Mininni

National Center for Atmospheric Research, P.O. Box 3000, Boulder, Colorado 80307
(Dated: February 14, 2017)

Planetary and stellar dynamos likely result from turbulent motions in magnetofluids with kinematic viscosities that are small compared to their magnetic diffusivities. Laboratory experiments are in progress to produce similar dynamos in liquid metals. This work reviews recent computations of thresholds in critical magnetic Reynolds number above which dynamo amplification can be expected for mechanically-forced turbulence (helical and non-helical, short wavelength and long wavelength) as a function of the magnetic Prandtl number P_M. New results for helical forcing are discussed, for which a dynamo is obtained at $P_M = 5 \times 10^{-3}$. The fact that the kinetic turbulent spectrum is much broader in wavenumber space than the magnetic spectrum leads to numerical difficulties which are bridged by a combination of overlapping direct numerical simulations and subgrid models of magnetohydrodynamic turbulence. Typically, the critical magnetic Reynolds number increases steeply as the magnetic Prandtl number decreases, and then reaches an asymptotic plateau at values of at most a few hundred. In the turbulent regime and for magnetic Reynolds numbers large enough, both small and large scale magnetic fields are excited. The interactions between different scales in the flow are also discussed.

PACS numbers: 47.65.+a; 47.27.Gs; 95.30.Qd

I. INTRODUCTION

Plasmas in stellar interiors and conducting fluids in planetary cores are characterized by a magnetic Prandtl number P_M (the ratio of the kinematic viscosity ν to the magnetic diffusivity η) much smaller than one. As a few examples, the magnetic Prandtl number in the solar convective region is estimated to be $P_M \approx 10^{-5} - 10^{-6}$ [1], and in the Earth's core $P_M \approx 10^{-5}$. Liquid sodium experiments are also characterized by small values of P_M.

While numerical simulations of dynamo action in these objects are available, the large values of the kinetic (R_V) and magnetic (R_M) Reynolds numbers forbid a study using realistic values of P_M. Simulations of the geodynamo [2] or the solar convective region [3] are often done for $P_M \sim 1$. While the proper separation of the kinetic and magnetic dissipation scales cannot be achieved in these simulations, values of P_M much smaller than one can be reached under more idealized conditions. Pseudospectral methods in periodic boxes give an excellent tool to study the behavior of magnetohydrodynamic (MHD) turbulence in the regime $P_M < 1$. The further assumption of incompressibility allows for an extra gain in computer power. Paralellized pseudospectral codes have reached for hydrodynamic turbulence resolutions of 4096^3 grid points, and Taylor Reynolds numbers of $R_\lambda \approx 1200$ [4]. These methods are conservative and nondispersive, being well suited for the exploration of turbulent flows in regimes hard to explore in the laboratory. And under some circumstances, the range of values of P_M can be extended using subgrid scale (SGS) models.

In this work, we review recent results from simulations of helical and non-helical dynamos at $P_M < 1$ using pseudospectral codes in periodic boxes [5, 6, 7]. To extend the range in P_M in the simulations, SGS models were used in these works. We discuss some of these models with particular emphasis in the Lagrangian Average MHD (LAMHD) equations [8, 9, 10, 11, 12]. In addition, and to validate results from SGS models, new results from direct numerical simulations (DNS) with resolutions of 1024^3 grid points are presented.

We focus on the properties of the magnetic field in the kinematic dynamo regime, when the intensity of the magnetic field is small and the effect of the Lorentz force can be neglected. In particular, we discuss the behavior of the threshold in R_M for dynamo action as P_M is decreased. That is to say, given a hydrodynamic state and an arbitrary small magnetic perturbation, what is the minimum value of R_M (or maximum value of η, in some convenient set of dimensionless units) to have a dynamo instability such that the system reaches after a finite time a magnetohydrodynamic steady state. Below this threshold, the magnetic perturbation is damped and the final state of the system is hydrodynamic.

Two flows have recently been studied in this context: the flow resulting from Taylor-Green forcing [5, 6], and the result of Roberts forcing [7, 13]. The first case corresponds to a flow with no net helicity that gives large scale dynamo action, while the former studies are for a helical flow where only small scale dynamo action is permitted by introducing mechanical energy in the largest available scale. In a different context, for isotropic, homogeneous, and delta-correlated in time external forcing, the problem has also been studied in Refs. [14, 15]. In addition to reviewing this results, we compare them against new simulations using Arn'old-Childress-Beltrami (ABC) forcing with energy injection at intermediate scales. This is a helical case where large scale magnetic amplification is allowed. For this forcing, values of P_M down to 5×10^{-3} are reached. The results obtained for such a low value of P_M are expected to be of relevance for astrophysical and geophysical applications, as well as for laboratory dynamos.

For all cases where a large scale flow is present, dynamo action is observed to persist at the smallest values of P_M that can be reached. Moreover, for values of P_M smaller than ~ 0.1 an independence of the threshold with P_M is observed. While for the Taylor-Green (non-helical) forcing and the Roberts forcing (helical, but with magnetic amplification only at small scales) a sharp increase in the critical parameter is observed before reaching the asymptotic regime, in the ABC case almost no such increase is found.

The structure of the paper is as follows. In Sec. II we present the equations, and the several forcing functions used. We also describe the code and the SGS models. Section III discusses the thresholds for dynamo action for the several flows, and Sec. IV discusses the role played by the different scales in the problem. Finally, Sec. V presents the conclusions.

II. EQUATIONS

A. The MHD equations

In dimensionless Alfvénic units, the incompressible MHD equations are

$$\frac{\partial \mathbf{v}}{\partial t} + \mathbf{v} \cdot \nabla \mathbf{v} = -\nabla \mathcal{P} + \mathbf{j} \times \mathbf{B} + \nu \nabla^2 \mathbf{v} + \mathbf{f}, \quad (1)$$

$$\frac{\partial \mathbf{B}}{\partial t} + \mathbf{v} \cdot \nabla \mathbf{B} = \mathbf{B} \cdot \nabla \mathbf{v} + \eta \nabla^2 \mathbf{B}, \quad (2)$$

with $\nabla \cdot \mathbf{v} = \nabla \cdot \mathbf{B} = 0$. Here $\mathbf{v}$ is the velocity field, and $\mathbf{B}$ is the magnetic field, related to the electric current density $\mathbf{j}$ by $\mathbf{j} = \nabla \times \mathbf{B}$. $\mathcal{P}$ is the normalized pressure-to-density ratio, obtained by solving the Poisson equation that results from taking the divergence of Eq. (1) and using the condition $\nabla \cdot \mathbf{v} = 0$.

In Eq. (1) $\mathbf{f}$ is an external force. Since in the incompressible framework we lack the usual energy sources in astrophysics and geophysics (e.g. thermal convection), we will set $\mathbf{f}$ to generate a large scale flow, and let the instabilities of the flow generate turbulent fluctuations. The expressions for $\mathbf{f}$ considered are discussed in the following subsection.

Equations (1) and (2) are solved using a standard pseudospectral method [16, 17] in a three dimensional periodic box. The code uses projection into the Fourier base to compute spatial derivatives, and Runge-Kutta of adjustable order to evolve the equations in time. The 2/3-rule for dealiasing is used. As a result, if N grid points are used in each direction, the maximum wavenumber solved by the code is $k_{max} = N/3$. To make use of parallel computers, the three dimensional Fourier transform has to be parallelized efficiently, using a methodology as described e.g. in Refs. [18, 19].

All Reynolds numbers discussed are based on the flow integral scale

$$L = 2\pi \int E_V(k) k^{-1} \, dk / E_V \quad (3)$$

where $E_V(k)$ is the kinetic energy spectrum, and $E_V = \int E_V(k) dk$ is the total kinetic energy. Given the r.m.s. velocity U, the kinetic Reynolds number is $R_V = LU/\nu$ and the magnetic Reynolds number is $R_M = LU/\eta$. The magnetic Prandtl number is $P_M = R_M/R_V$. We also define the large scale eddy turnover time as $T = L/U$. The kinetic and magnetic dissipation wavenumbers in the turbulent regime are given by $k_\nu = (\epsilon/\nu^3)^{1/4}$ and $k_\eta = (\epsilon/\eta^3)^{1/4}$ respectively, where ϵ is the energy injection rate. In all simulations, these wavenumbers were smaller than the maximum resolved wavenumber k_{max}.

The strategy is to turn on the forcing at $t = 0$ and allow the code to run for a time as a hydrodynamic code, with the magnetic field set to zero. Once a stationary state is reached, the magnetic field is seeded with randomly-chosen Fourier coefficients and allowed to amplify or decay.

B. External forcing

Several expressions for the external forcing were studied in the context of dynamo action. Refs. [5, 6] considered Taylor-Green [20] forcing

$$\mathbf{f}_{\mathrm{TG}} = [\sin(k_{\mathrm{TG}}x)\cos(k_{\mathrm{TG}}y)\cos(k_{\mathrm{TG}}z)\hat{x} - \\ - \cos(k_{\mathrm{TG}}x)\sin(k_{\mathrm{TG}}y)\cos(k_{\mathrm{TG}}z)\hat{y}], \quad (4)$$

with wavenumber $k_{\mathrm{TG}} = 2$ (this election gives a peak in the kinetic energy at $k \approx 3$). If Eq. (4) is used as an initial condition for the velocity field $\mathbf{v}$, it is found that the flow is not a solution of the Euler's equation and though highly symmetric, it leads to the rapid development of small spatial scales. The forcing is also non-helical, in the sense that $\mathbf{f}_{\mathrm{TG}} \cdot \nabla \times \mathbf{f}_{\mathrm{TG}}$ is zero at every point in space. Helical fluctuations can however appear at scales smaller than the forcing scale.

Ref. [7, 13] considered the Roberts flow [21, 22] as the expression for the external force $\mathbf{f}$:

$$\mathbf{f}_{\mathrm{R}} = [g\sin(k_{\mathrm{R}}x)\cos(k_{\mathrm{R}}y)\hat{x} - g\cos(k_{\mathrm{R}}x)\sin(k_{\mathrm{R}}y)\hat{y} + \\ + 2f\sin(k_{\mathrm{R}}x)\sin(k_{\mathrm{R}}y)\hat{z}], \quad (5)$$

with the choice $k_{\mathrm{R}} = 1$. Since in that case mechanical energy is injected in the largest available scale, magnetic excitations can only grow at scales smaller than the energy injection scale. The coefficients f and g are arbitrary and their ratio determines the extent to which the flow excited will be helical. We will concentrate here upon the case $f = g$. In this case, the forcing injects helicity in the flow, although not maximally. If used as an initial condition, the velocity field is an exact solution of Euler's equation. As a result, the development of small scale fluctuations only takes place above a certain threshold in the kinetic Reynolds number R_V. For values of R_V smaller than this threshold, there is an exact laminar solution of the hydrodynamic equations given by $\mathbf{v} = \mathbf{f}/(\nu k_{\mathrm{R}}^2)$.

We compare the results from these two forcing functions with the ABC forcing

$$\mathbf{f}_{\text{ABC}} = \{[B\cos(k_{\text{ABC}}y) + C\sin(k_{\text{ABC}}z)]\,\hat{x} +$$
$$+ [A\sin(k_{\text{ABC}}x) + C\cos(k_{\text{ABC}}z)]\,\hat{y} +$$
$$+ [A\cos(k_{\text{ABC}}x) + B\sin(k_{\text{ABC}}y)]\,\hat{z}\}, \quad (6)$$

with $k_{\text{ABC}} = 3$, and $A = 0.9$, $B = 1$, and $C = 1.1$. Previous results for $P_M < 1$ have been reported in Refs. [23, 24], although no systematic study of the effect of lowering P_M was done.

The ABC flow is maximally helical, and the election of k_{ABC} allows for the growth of magnetic energy at scales larger than the energy injection scale. As for the Roberts flow, the ABC flow is also an exact solution of the Euler's equation, and turbulent fluctuations are generated as the result of a hydrodynamic instability at values of R_V larger than a certain threshold. The particular election of the parameters A, B, and C is done to break the symmetry of the flow and reduce the value of the hydrodynamic threshold [24, 25].

C. Subgrid models of MHD turbulence

As the value of P_M is lowered down, the separation between the Ohmic and viscous dissipation scales increases. As a result, the velocity field has more small scale structure than the magnetic field. This imposes a stringent limit on the smallest P_M that can be reached using DNS. At some point, the small scales in the flow cannot be solved anymore, and some form of SGS modeling is required.

While SGS models of hydrodynamic turbulence have a rich history, models for MHD flows are still in their infancy (see e.g. [26]). One of the main difficulties in MHD is that hypotheses often made in hydrodynamics (e.g. locality of interactions in Fourier space) are not necessarily true for magnetofluids. The general expression of the MHD energy spectrum is not known. And several regimes can be expected according to whether the system is mechanically or magnetically forced, whether the fields are statistically aligned or not, etc.

In this work we will focus on the LAMHD equations (or MHD α-model). The hydrodynamic α-model (see e.g [8, 9] and references therein) was validated against simulations in Ref. [27]. It differs from large eddy simulations (LES) in that the filter is applied to the Lagrangian of the ideal fluid, and as a result Hamiltonian properties of the system are preserved. It was extended to ideal MHD [8, 9], and tested against DNS of MHD turbulence [11, 12]. In the context of magnetoconvection, the LAMHD equations were also studied in Ref. [28]. In the incompressible case, the LAMHD equations are

$$\frac{\partial \mathbf{v}}{\partial t} + \mathbf{u}_s \cdot \nabla \mathbf{v} = -v_j \nabla u_s^j - \nabla \widetilde{\mathcal{P}} + \mathbf{j} \times \mathbf{B}_s$$
$$+ \nu \nabla^2 \mathbf{v} + \mathbf{f}, \quad (7)$$
$$\frac{\partial \mathbf{B}_s}{\partial t} + \mathbf{u}_s \cdot \nabla \mathbf{B}_s = \mathbf{B}_s \cdot \nabla \mathbf{u}_s + \eta \nabla^2 \mathbf{B}.. \quad (8)$$

The pressure $\widetilde{\mathcal{P}}$ is to be determined, as before, from the relevant Poisson equation. The energy in this system is given by $E = \int (\mathbf{v} \cdot \mathbf{u}_s + \mathbf{B} \cdot \mathbf{B}_s)/2\,d^3x$. The subindex s denotes smoothed fields, related to the unsmoothed fields by

$$\mathbf{v} = \left(1 - \alpha^2 \nabla^2\right) \mathbf{u}_s \quad (9)$$
$$\mathbf{B} = \left(1 - \alpha^2 \nabla^2\right) \mathbf{B}_s. \quad (10)$$

In the context of the dynamo at low P_M, some others SGS models have been used. Ref. [5] used a modified LES [29] where only the velocity field at scales smaller than the magnetic diffusion scale was modeled using a turbulent effective viscosity dependent on the wavenumber. A similar SGS model has been used in Ref. [15] to study dynamo action with delta-correlated in time random forcing, but with the expression of the effective viscosity based on the Smagorinsky-Lilly model. Ref. [15] also used hyperviscosity, although it should be remarked that this method is known to give wrong growth rates for the magnetic energy in the anisotropic case [30].

III. BEHAVIOR OF THE DYNAMO WITH P_M

Figure 1 (bottom panel) shows the critical magnetic Reynolds number R_M^c as a function of R_V for Taylor-Green forcing. Crosses connected with solid lines are obtained using DNS, while crosses connected with dotted lines are from LAMHD simulations (the largest resolution used by each method was of 512^3 grid points). An overlap of the two methods for three values of R_V was used to verify the SGS model. In Ref. [5] higher values of R_V were reached for this flow using LES.

Above the threshold, magnetic field excitations are amplified exponentially until the system reaches a fully developed MHD regime. Below the threshold, magnetic field perturbations are damped and the system reaches after long times a hydrodynamic regime.

The threshold is obtained from simulations in the following way: in the steady state of a hydrodynamic simulation at a given value of R_V, a small magnetic field is introduced and several simulations varying R_M are carried. In each MHD simulation, the exponential growth or decay rate $\sigma = d\log E_M/dt$ of the magnetic energy is measured. The value of R_M for which $\sigma = 0$ defines R_M^c. In practice, R_M^c is bounded between two values of R_M that give positive and negative σ, and the actual value of R_M^c is obtained from a best fit to the σ vs. R_M curve (see e.g. Refs. [5, 6]). This procedure gives the value of R_M^c with an error of the order of 10%.
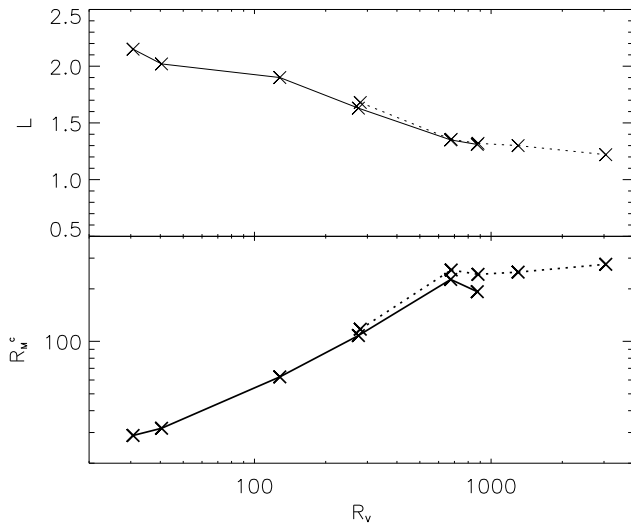
FIG. 1: Integral lengthscale of the flow as a function of R_V (above), and critical magnetic Reynolds for dynamo action R_M^c as a function of R_V (below) for the Taylor-Green forcing. Crosses connected with solid lines are obtained from DNS, while crosses connected with dotted lines are obtained using the LAMHD equations.

Figure 1 (top panel) also shows the flow integral scale as R_V is increased. This scale is measured in the steady state of the hydrodynamic run that preceeds the MHD simulations. At low R_V the flow is laminar and L is close to the forcing scale $2\pi/k_{\mathrm{TG}}$. However, as R_V is increased, more and more small scale excitations appear in the flow, and L decreases. For $R_V \approx 1000$, the system has reached a fully turbulent regime with a Kolmogorov's energy spectrum. For larger values of R_V, L changes slowly. Note that R_M^c is anti-correlated with L. As R_V increases, R_M^c grows sharply. But for $R_V \approx 1000$ ($P_M \approx 0.3$) the threshold in R_M^c settles around 300, and the system seems to reach an asymptotic regime.

The same quantities are shown in Fig. 2 for the Roberts forcing (see also Ref. [7]). In this case, the external forcing is an exact solution of the Euler's equation, and for $R_V \lesssim 100$ the flow is hydrodynamically stable. Between $R_V \approx 100$ and $R_V \approx 1000$ the flow displays hydrodynamic oscillations, and for $R_V \gtrsim 1000$ the flow reaches a hydrodynamic turbulent regime with a Kolmogorov's power law in the inertial range. As a result of these instabilities, the characteristic scale of the flow changes twice sharply. In the laminar regime $L \approx 2\pi/k_{\mathrm{R}}$. Then L decreases and remains approximately constant in the oscillatory regime ($400 \lesssim R_V \lesssim 1000$), and finally has a second sharp decrease ($R_V \approx 1000$) as turbulence develops. The threshold for dynamo action shows again an anti-correlation with L, and two sharp increases in R_M^c as a function of R_V are observed as L changes. In the turbulent regime ($R_V \approx 1000$), an asymptotic value of R_M^c seems again to be reached. In this case, only DNS
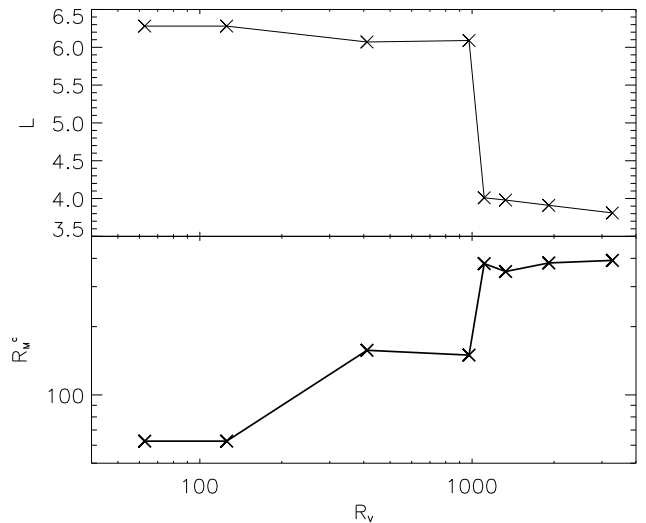

FIG. 2: Integral lengthscale of the flow as a function of R_V (above), and R_M^c as a function of R_V (below) for Roberts forcing.
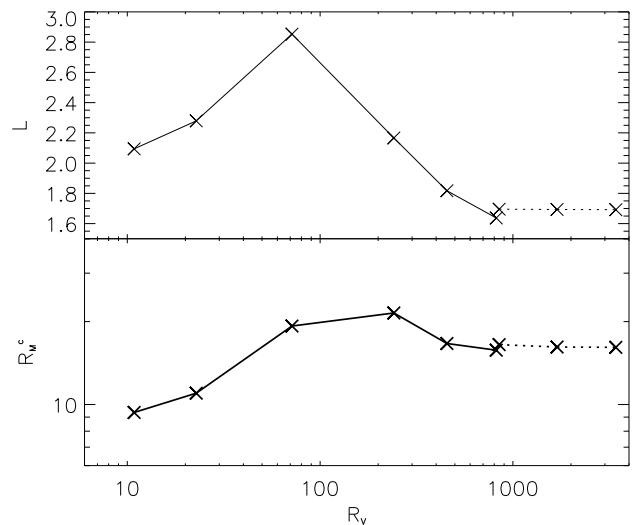

FIG. 3: Integral lengthscale of the flow as a function of R_V (above), and R_M^c as a function of R_V (below) for ABC forcing. Crosses connected with solid lines are obtained from DNS, while crosses connected with dotted lines are obtained using the LAMHD equations.

was used.

Figure 3 shows the threshold and integral scale as a function of R_V for ABC forcing. As mentioned in the previous section, this is a helical flow with energy injection at intermediate scales, and as a result large scale dynamo action can take place. As for Taylor-Green forcing, crosses connected with solid lines are obtained from DNS, while crosses connected with dotted lines are obtained from LAMHD simulations. There is an anti-correlation
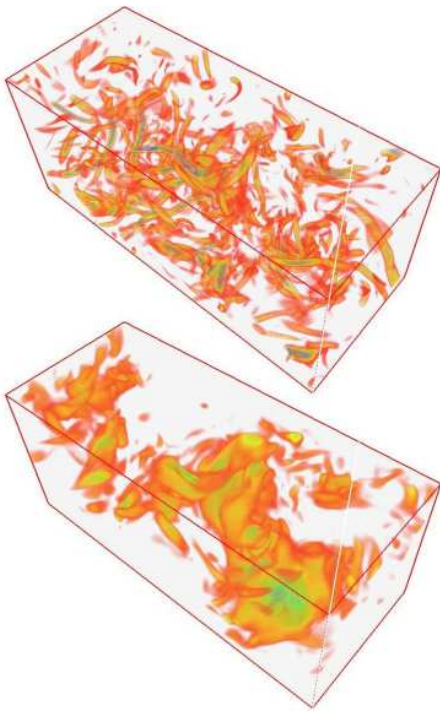
FIG. 4: Volume render of enstrophy density (above) and square current density (below) in a small region of a simulation with $P_M = 5 \times 10^{-2}$ and ABC forcing.

FIG. 5: Spectrum of kinetic energy (thick line) and magnetic energy (thin line) in a 1024^3 simulation with Taylor-Green forcing ($P_M = 0.1$ and $R_M = 400$). The spectrum of magnetic energy has been multiplied by 10. Kolmogorov's and Kazanstsev's power laws are shown as a reference.

between L and R_V, but it is less clear than in the previous flows. In the laminar case ($R_V \approx 10$) the integral scale is close to $2\pi/k_{ABC}$, while in the turbulent regime ($R_V \approx 1000$) R_M^c is larger and L is smaller. However, there is an intermediate range where L grows together with R_M^c. The increase of L in this intermediate regime is associated with the development of chaotic trajectories connecting several ABC cells as the flow bifurcates. The hydrodynamic bifurcations and subsequent generation of small scales (breaking the infinite time correlation of the laminar flow) also gives rise to an enhanced diffusivity that in turns increases R_M^c.

When compared with the previous flows, there are two striking differences in the amplitude of R_M^c as a function of R_V. First, the thresholds at high R_V are reduced by one order of magnitude. Second, there is only a small dependence of R_M^c with R_V. As the flow destabilizes and develops turbulence ($R_V \approx 100$) the threshold changes from $R_M^c \approx 10$ to $R_M^c \approx 20$, while in the previously discussed flows the increase is by a factor of 10. After that, R_M^c drops and finally stabilizes. Note that the smallest magnetic Prandtl number of $P_M \approx 5 \times 10^{-3}$ was reached for this flow.

Figure 4 shows renders of the enstrophy density and mean square current in a small box in a DNS using ABC forcing and $P_M = 5 \times 10^{-2}$. The scale separation between the kinetic and magnetic diffusion scales is evident. While the velocity field displays thin and elongated vortex tubes, the structures in the magnetic field are thicker.
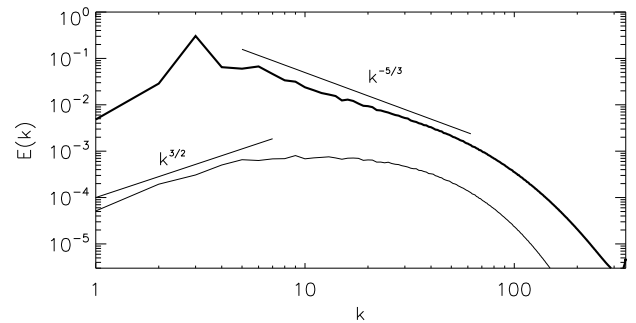
In simulations without large scale flows [14, 15] no asymptotic regime for low P_M has been found so far. As R_V is increased and the system develops turbulent fluctuations, R_M^c grows to values much larger than the ones obtained here. From the numerical results, it is not clear whether an asymptotic regime will be reached or R_M^c will continue growing. However, theoretical arguments [31] suggest that R_M^c should be constant for values of R_V large enough. From the comparison with the cases studied here and the anti-correlation found between L and R_M^c, it is clear that the presence of a large scale flow (helical or not) plays a crucial role in the development of the asymptotic regime at relatively small values of R_V and R_M.

IV.   SCALE INTERACTIONS

The results presented in the previous section raise the question of what are the effects of turbulence, beyond increasing the value of R_M^c. Does dynamo action only take place at large scales when $P_M < 1$, or can turbulent fluctuations also amplify small scale magnetic fields? By small scales, we refer here to scales smaller than the flow integral scale but larger than the magnetic diffusion scale.

Figure 5 shows the kinetic and magnetic energy spectrum in the kinematic regime of a 1024^3 DNS using Taylor-Green forcing ($P_M = 0.1$ and $R_M = 400$). The magnetic energy spectrum peaks at scales smaller than the flow integral scale, and at intermediate scales the spectrum is approximately flat. At large scales, a slope compatible with Kazantsev's spectrum [32] is observed, although it should be noted that the hypothesis used by Kazantsev do not apply to this case. In Ref. [5] it was shown that the peak in the magnetic energy spectrum moves to small scales as R_V is increased.

The role played by the different scales in the flow is further clarified by examining the energy transfer functions.
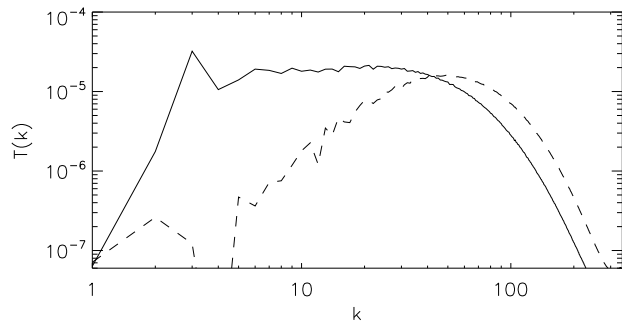
FIG. 6: Transfer functions $-T_L(k)$ (solid line) and $T_M(k)$ (dashed line) in the 1024^3 simulation with Taylor-Green forcing.
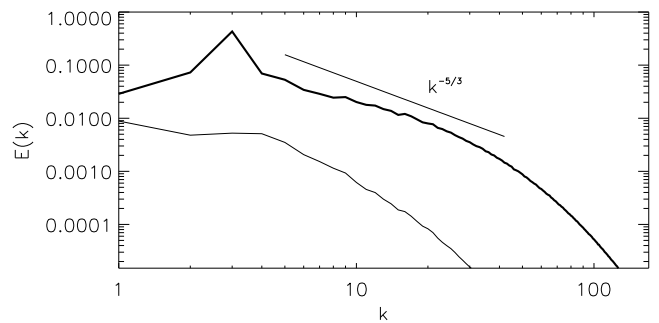

FIG. 7: Spectrum of kinetic energy (thick line) and magnetic energy (thin line) in a 512^3 simulation with ABC forcing ($P_M = 1.5 \times 10^{-2}$ and $R_M = 40$). The spectrum of magnetic energy has been multiplied by 10.

From Eqs. (1) and (2), the transfers

$$T_L(k) = \int \widehat{\mathbf{v}}_{\mathbf{k}}^* \cdot \left(\widehat{\mathbf{j} \times \mathbf{B}}\right)_{\mathbf{k}} d\Omega_{\mathbf{k}}, \qquad (11)$$

$$T_M(k) = \int \widehat{\mathbf{B}}_{\mathbf{k}}^* \cdot \nabla \times \left(\widehat{\mathbf{v} \times \mathbf{B}}\right)_{\mathbf{k}} d\Omega_{\mathbf{k}}, \qquad (12)$$

can be defined (see e.g. Ref. [6]). The asterisk denotes complex conjugate, the hat Fourier transform, the subindex denotes the amplitude of the mode with wavevector $\mathbf{k}$, and $d\Omega_{\mathbf{k}}$ is the element of surface of the sphere of radius k in Fourier space. When negative, $T_L(k)$ represents energy given by the velocity field at the wavenumber k to the magnetic field at all scales. Positive $T_M(k)$ represents energy received by the magnetic field at wavenumber k from the velocity field at all scales, and from the direct cascade of energy. The detailed shell-to-shell energy transfer in the kinematic dynamo has been studied in Ref. [33].

Figure 6 shows the transfer functions for the 1024^3 DNS with Taylor-Green forcing. The magnetic field receives energy from the velocity field in all scales in the inertial range (note that T_L has constant amplitude from $k \approx 3$ up to $k \approx 40$). As a result, for this forcing both the large scale flow and the turbulent fluctuations give energy to the magnetic field. On the other hand, $T_M(k)$ peaks at $k \approx 60$. This suggests that the dynamo process is non-local in Fourier space. Other indications of non-local interactions from simulations were obtained in Ref. [34], and in simulations of dynamo action at large P_M [35], although direct verification of the nonlocality in MHD turbulence was not obtained until recently [36, 37].

Similar results were obtained for Roberts forcing [7]. In that case, a magnetic energy spectrum peaking at small scales and an approximately flat $T_L(k)$ transfer function at small scales were observed.

The results for ABC forcing are different. Figure 7 shows the kinetic and magnetic energy spectrum in a 512^3 DNS with $P_M = 1.5 \times 10^{-2}$ and $R_M = 40$. In this case,

the magnetic energy spectrum peaks at $k = 1$, and no peak is observed at scales smaller than the integral scale of the flow. Moreover, the magnetic energy spectrum drops fast. The transfer $T_L(k)$ (Fig. 8) shows that most of the amplification is done by the large scale flow at $k = 3$, and the turbulent fluctuations seem to give only a small contribution to the dynamo. $T_M(k)$ shows that most of the energy is received by the magnetic field at large scales, and it drops as $T_L(k)$ at small scales.

The reason for this behavior can be understood as follows. For ABC forcing, R_M^c is of the order of a few tens, even in the fully turbulent regime. As a result, a dynamo simulation just above threshold has small R_M, and small magnetic scales are damped so fast that no inertial range can develop in the magnetic energy spectrum. As a result, the magnetic field is only amplified by the large scale flow and grows at larger scales. Since there is no dynamo source at scales smaller than the flow integral scale, the small scales are only fed by the direct cascade of energy and the magnetic energy spectrum cannot peak at these scales.

However, if a simulation using ABC forcing is done at larger values of R_M, dynamo amplification by the small scales is recovered and similar features than for Taylor-Green forcing are obtained [23, 33]. This situation should be the one that prevails in astrophysics.

V. CONCLUSIONS

We reviewed results of dynamo action at low magnetic Prandtl number [5, 6, 7] for several mechanical forcing functions, including helical and non-helical flows, as well as small and large scale dynamo action. For all cases where a large scale flow is present, a similar behavior is obtained in the threshold for dynamo action: as R_V is increased (or P_M decreased), the value of R_M^c increases sharply as turbulence develops and finally reaches an asymptotic regime independent of the value of P_M. The
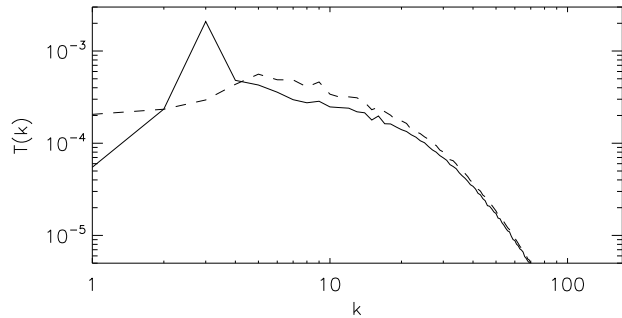
FIG. 8: Transfer functions $-T_L(k)$ (solid line) and $T_M(k)$ (dashed line) in the 512^3 simulation with ABC forcing.

critical magnetic Reynolds is smaller than for the other two flows by one order of magnitude. Also, only a twofold increase in R_M^c is observed as turbulence develops (in contrast to a tenfold increase for the other flows). As a result, dynamo simulations close to the threshold do not show small scale amplification (down to $P_M = 5 \times 10^{-3}$), and only the large scale flow is responsible for the large scale dynamo action. However, as the value of R_M is increased, as is expected for astrophysical and geophysical flows, small scale amplification in the kinematic regime is recovered.

Although the conditions in our simulations are idealized, we believe the existence of an asymptotic regime for $P_M < 1$ has profound implications for laboratory experiments and modeling of astrophysical and geophysical dynamos. In most of these cases, a large scale flow (such as differential rotation) and turbulent fluctuations are known to be present.

large scale flow plays an important role in the establishment of the asymptotic behavior, as shown by the anticorrelation between the characteristic length of the flow and R_M^c. As turbulence develops, the laminar flow creates small scales through hydrodynamic instabilities, and the large scale laminar flow loses its infinite correlation time. Then, both the large and small scale velocity fields amplify the magnetic field, giving rise to the asymptotic regime.

New results from simulations with ABC forcing present a distinctive behavior. Having the flow maximum kinetic helicity and permitting large scale dynamo action, the

[1] E.N. Parker, *Cosmical Magnetic Fields* (Clarendon Press, New York, 1979)
[2] G.A. Glatzmaier, R.S. Coe, L. Hongre, and P.H. Roberts, Nature **401**, 885 (1999).
[3] F. Cattaneo, Astrophys. J. **515**, 39 (1999).
[4] Y. Kaneda, T. Ishihara, M. Yokokawa, K. Itakura, and A. Uno, Phys. Fluids **15**, L21 (2003).
[5] Y. Ponty, P.D. Mininni, D.C. Montgomery, J.-F. Pinton, H. Politano, A. Pouquet, Phys. Rev. Lett. **94**, 164502 (2005).
[6] P.D. Mininni, Y. Ponty, D.C. Montgomery, J.-F. Pinton, H. Politano, A. Pouquet, Astrophys. J. **626**, 853 (2005).
[7] P.D. Mininni and D.C. Montgomery, Phys. Rev. E, in press (2005).
[8] D.D. Holm, Phys. D **170**, 256 (2002).
[9] D.D. Holm, Chaos **12**, 518 (2002).
[10] D.C. Montgomery and A. Pouquet, Phys. Fluids **14**, 3365 (2002).
[11] P.D. Mininni, D.C. Montgomery, A. Pouquet, Phys. Fluids **17**, 035112 (2005).
[12] P.D. Mininni, D.C. Montgomery, A. Pouquet, Phys. Rev. E **71**, 046304 (2005).
[13] F. Feudel, M. Gellert, S. Rudiger, A. Witt, and N. Seehafer, Phys. Rev. E **68**, 046302 (2003).
[14] N.E.L. Haugen, A. Brandenburg, and W. Dobler, Phys. Rev. E **70**, 016308 (2004).
[15] A.A. Schekochihin, N.E.L. Haugen, A. Brandenburg, S.C. Cowley, J.L. Maron, and J.C. McWilliams, Astro-

phys. J. **625**, L115 (2005).
[16] S.A. Orszag and G.S. Patterson, Jr., Phys. Rev. Lett. **28**, 76 (1972).
[17] C. Canuto, M.Y. Hussaini, A. Quarteroni, and T. A. Zang, *Spectral methods in fluid dynamics* (Springer-Verlag, New York, 1988).
[18] P. Dmitruk, L.-P. Wang, W.H. Matthaeus, R. Zhang, and D. Seckel, Parallel Comp. **27**, 1921 (2001).
[19] D.O. Gómez, P.D. Mininni, and P. Dmitruk, Phys. Scripta, **T116**, 123 (2005).
[20] G.I. Taylor and A.E. Green, A.E., Proc. Roy. Soc. Lond. A **158**, 499 (1937).
[21] G. O. Roberts, Phil. Tran. R. Soc. Lond. A **271**, 1216 (1972).
[22] M.L. Dudley and R.W. James, Proc. Roy. Soc. Lond. A **425**, 1869 (1989).
[23] A. Brandenburg, Astrophys. J. **550**, 824 (2001).
[24] V. Archontis, S.B.F. Dorch, and Å. Nordlund, Astron. Astr. **410**, 759 (2003).
[25] O. Podvigina and A. Pouquet, Phys. D **75**, 471 (1994).
[26] W.-C. Müller and D. Carati, Comp. Phys. Comm. **147**, 544 (2002).
[27] S.Y. Chen, D.D. Holm, L.G. Margolin, and R. Zhang, Phys. D **133**, 66 (1999).
[28] C.A. Jones and P.H. Roberts, "Turbulence models plane layer dynamos," in *Fluid dynamics and dynamos in astrophysics and geophysics*, edited by A.M. Soward, C.A. Jones, D.W. Hughes, and N.O. Weiss (CRC Press, Boca

Raton, 2005).

[29] Y. Ponty, H. Politano, and J.F. Pinton, Phys. Rev. Lett. **92**, 144503 (2004).

[30] F.H. Grote, F.H. Busse, and A. Tilgner, Geophys. Res. Lett. **27**, 2001 (2000).

[31] S. Boldyrev and F. Cattaneo, Phys. Rev. Lett. **92**, 144501.

[32] A.P. Kazantsev, Sov. Phys. JETP **26**, 1031 (1968).

[33] P.D. Mininni, A. Alexakis, and A. Pouquet, Phys. Rev. E **72**, 046302 (2005).

[34] S. Kida, S. Yanase, and J. Mizushima, Phys. Fluids A **3**, 457 (1991).

[35] A.A. Schekochin, S.C. Cowley, S.F. Taylor, J.L. Maron, and J.C. McWilliams, Astrophys. J. **612**, 276 (2004).

[36] O. Debliquy, M.K. Verma, and D. Carati, Phys Plasmas, **12**, 042309 (2005).

[37] A. Alexakis, P.D. Mininni, and A. Pouquet, Phys. Rev. E **72**, 046301 (2005).